Interface characterization of Mo/Si multilayers

Jiaoling Zhao (赵娇玲)[1,2], Hongbo He (贺洪波)[1,*], Hu Wang (王 虎)[1,2], Kui Yi (易 葵)[1], Bin Wang (王 斌)[1,2], and Yun Cui (崔 云)[1]

[1]*Shanghai Institute of Optics and Fine Mechanics, Chinese Academy of Sciences, Shanghai 201800, China*

[2]*University of Chinese Academy of Sciences, Beijing 100049, China*

**Corresponding author: hbhe@siom.ac.cn*

Received March 2, 2016; accepted May 24, 2016; posted online June 30, 2016

Complementary analysis techniques are applied in this work to study the interface structure of Mo/Si multilayers. The samples are characterized by grazing incident x-ray reflectivity, x-ray photoelectron spectroscopy, high-resolution transmission electron microscopy, and extreme ultraviolet reflectivity. The results indicate that the layer thickness is controlled well with small diffusion on the interface by forming $MoSi_2$. Considering $MoSi_2$ as the interface composition, simulating the result of our four-layer model fits well with the measured reflectivity curve at 13.5 nm.

OCIS codes: 340.7480, 230.4170.

doi: 10.3788/COL201614.083401.

Multilayer coating reflectors are used as major components in extreme ultraviolet (EUV) lithography[1], soft x-ray microscopy[2], and x-ray astronomy[3]. Mo/Si multilayer coatings are the preferred components in EUV lithography systems, which require sharp interface and thermal stability to improve the optical performance. Usually Mo/Si multilayer coatings shrink considerably after annealing, independently of the interface structure. Therefore, diffusion barrier layers such as C and B_4C[4], or different material pairs such as Mo_2C/Si or $MoSi_2$/Si[5], are usually preferred for high temperature stability. In order to realize the sharp interface, interface roughness and interface diffuseness have been recognized as two main aspects to be pursued. Recently, much work has been done to avoid the interface imperfections, such as deposition rate[6], thickness uniformity[7], and interface engineering[8–11]. The secondary ion mass spectrometry technique indicated that the interface roughness of the Si-on-Mo layer was varying from 1.1 to 2.2 nm[9]. Although the interlayer composition of the Mo-Si interface has been studied by many researchers, the nature of phase formation at both interlayers remains an open question[11]. The interface issues, such as compositions on the EUV coatings deposited by magnetron sputtering method, required detailed analysis. Moreover, combining the interlayer formation with the reflective spectrum is still required to build the optical model including the interface, which is essential for the further design and improvement of EUV coatings. In this study, interlayer composition of Mo/Si multilayer coatings fabricated by the magnetron sputtering method is investigated in detail with x-ray photoelectron spectroscopy (XPS). The proposed composition is supported by grazing incident x-ray reflectivity (GIXRR), high-resolution transmission electron microscopy (HRTEM), and reflective spectrum.

Mo/Si multilayers with an optimized structure [Sub |Si(Mo/Si)^{40}| Air] are deposited on Si (100) substrates by the magnetron sputtering method. The multilayer design and reflectivity calculation methods are similar to the IMD program[12]. The base pressure is 8.5×10^{-5} Pa and the working gas is argon at a pressure of 0.1 Pa. Mo (2.8 nm) and Si (4.2 nm) are alternately deposited on the substrates to fabricate the Mo/Si multilayers. The values in parentheses indicate the designed thicknessthat are determined by the deposition rate and time.

GIXRR measurements performing on a PANalytical Empyrean reflectometer with Cu-Kα (0.154 nm) radiation are generally used to characterize multilayer structures. XPS is used to examine the surface and interface compositions with a Thermo Scientific K-Alpha XPS instrument equipped with a monochromatic Al Kα x-ray source. Base pressure during analysis is about 4×10^{-9} mbar. For the depth profiling of the multilayer, an argon ion beam of an acceleration voltage of 400 V for theSi layer and 1 kV for the Mo layer are used to sputter the multilayer. The C ls, O ls, Si 2p, and Mo 3d peaks are recorded. Charging effects are corrected by referencing the binding energies to that of the adventitious C ls line at 284.5 eV. All binding energies obtained in this study are precise to within 0.2 eV.

The soft x-ray reflective spectrum around 13.5 nm is measured using the U26 beam line of the National Synchrotron Radiation Laboratory (NSRL) in Hefei.

HRTEM (Tecnai G2 F20 S-Twin) is used to observe the interlayer microstructures and determine the accurate layer thickness. For the high resolution image of the cross-sectional microstructure an operating voltage 200 kV is used under the bright-filed imaging.

The thicknesses of the periodic and individual layers in the Mo/Si multilayers are determined from GIXRR measured over the angular range of $\theta = 0°$–$5°$. The GIXRR produces a series of sharp peaks corresponding to the diffraction from the multilayer structure. First, the periodic thickness is obtained using Bragg's law with refractive correction $\sin^2\theta_m = (\lambda/2D)^2 m^2 + 2\bar{\delta}$, where θ_m is the glancing angle with corresponding diffraction order m, D is the periodic thickness, and $\bar{\delta}$ is the average refractive

correction factor. Then the thickness of the individual layers is analyzed by fitting the measured GIXRR data to calculations of the diffraction based on a four-layer mode with the pure Mo and Si layers and the two $MoSi_2$ interlayers[13]. It is performed with X′ Pert Reflectivity 1.3 software comprising a genetic fitting algorithm to find the vicinity of the global optimum of the fit and using the Marquardt–Levenberg algorithm to finally optimize the exact parameters[14], as shown in Fig. 1. Seven well-defined peaks indicate that the multilayer coatings possess a well-defined periodic structure with a period thickness of 70.6 3 Å. According to the fitting results, the structure of the multilayer period was determined to be Si (41.03 Å)/$MoSi_2$ (4.67 Å)/Mo (22.68 Å)/$MoSi_2$ (2.25 Å). Nevertheless, the thickness of two $MoSi_2$ interlayers for the Mo-on-Si and Si-on-Mo are different. Such asymmetry is attributed it being easier for Si to penetrate the amorphous-growing Mo layer than the textured Mo grains at the Mo-on-Si interface[15,16].

Depth-profile XPS measurements are carried out to investigate the chemical composition of the Mo/Si interface. Figure 2(a) shows the regional scan of the top Si layer for various etching times. Two peaks at the binding energy of 99.7 eV (Si) and 103.2 eV (SiO_2) are observed when the etching time is 0 s. As the etching time increases the SiO_x peak becomes weaker while the Si peak becomes stronger. In addition, the disappearance of the SiO_x peak indicates that the native oxide is formed only at the top Si surface. When the etching time increases from 120 to 165 s, the Si^{2-} species with a binding energy equal to that of $MoSi_2$ (99.4 eV)[17] is observed, which indicates the emergence of the Si-on-Mo interface. The concentration profile as a function of etching time is shown in Fig. 2(b). The atomic percent of Mo and Si are varying regularly with the etching time. The atomic percent of Si reaches the maximal value while the atomic percent of Mo is down to the minimum. The atomic percent of O is below 8% except the first 50 s, which indicates that only the very top surface is oxidized. As shown in Fig. 2(b), the Si-on-Mo interlayer emerges from 100 to 150 s and the Mo-on-Si interlayer emerges from 350 to 400 s.

To further study, the regional XPS scan spectra of Si 2p and Mo 3d on both the Si-on-Mo interface and the Mo-on-Si interface are measured and analyzed in

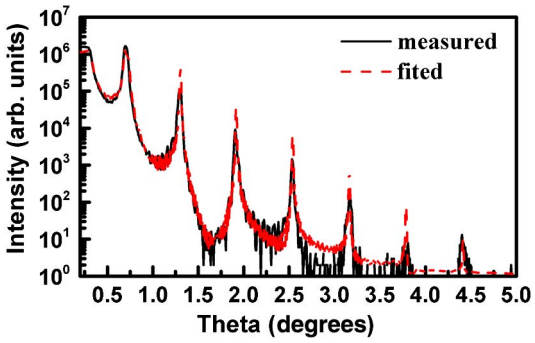

Fig. 1. Measured and fitted curve of GIXRR results.

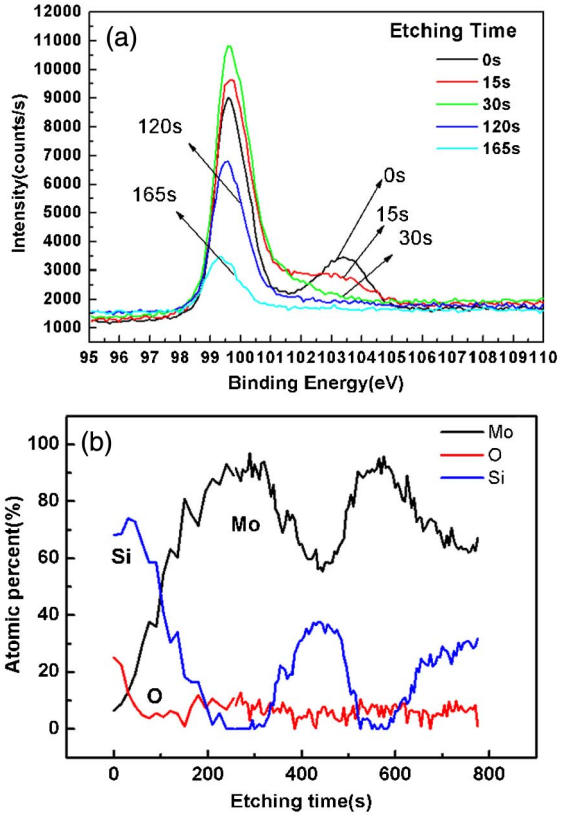

Fig. 2. (a) Regional XPS scan of the top Si layer for various etching times; (b) in-depth concentrate on the profile of the Mo/Si multilayer.

detail. The Si 2p, Mo $3d_{3/2}$, and Mo $3d_{5/2}$ lines corresponding to binding energies of 99.7, 230.9, and 227.7 eV are used in this study. $MoSi_2$, Mo_3Si, Mo_5Si_3, SiO_x, and MoO_x are taken into account during the fitting. The fitting curves are shown together with the measured values in Fig. 3. Fitting results of both Si 2p and Mo 3d are listed in Table 1.

As shown in Fig. 3, peak shift is observed for both Si 2p and Mo 3d spectra due to the formation of new compounds. The peak shift direction is the same as those reported for $MoSi_2$[18,19], but the binding energy values of Si 2p and Mo 3d for $MoSi_2$ are different. This could be related to the different fabrication method and measured environments.

The peak position of the Si 2p spectrum changes from 99.7 to 99.4 eV at the Si-on-Mo interface [Fig. 3(a)] and the peak position of the Mo spectrum ($3d_{5/2}$) changes from 227.70 to 228.09 eV [Fig. 3(b)]. The peak positions of the Si 2p spectrum and the Mo 3d spectrum (Mo $3d_{5/2}$) are 99.4 eV [Fig. 3(c)] and 228.11 eV [Fig. 3(d)], respectively. Si^{2-} from $MoSi_2$ and pure Si mainly contribute to the fitted Si 2p spectrum. Mo^{4+} from $MoSi_2$ and pure Mo mainly contribute to the fitted Mo 3d spectrum. According to the fitting results, $MoSi_2$ is the majority compound at the Mo/Si interfaces while SiO_x(103.38 eV) and MoO_x(231.9 eV) deviate significantly from the measured data. It is obvious that the SiO_x and MoO_x do not exist on both interfaces,

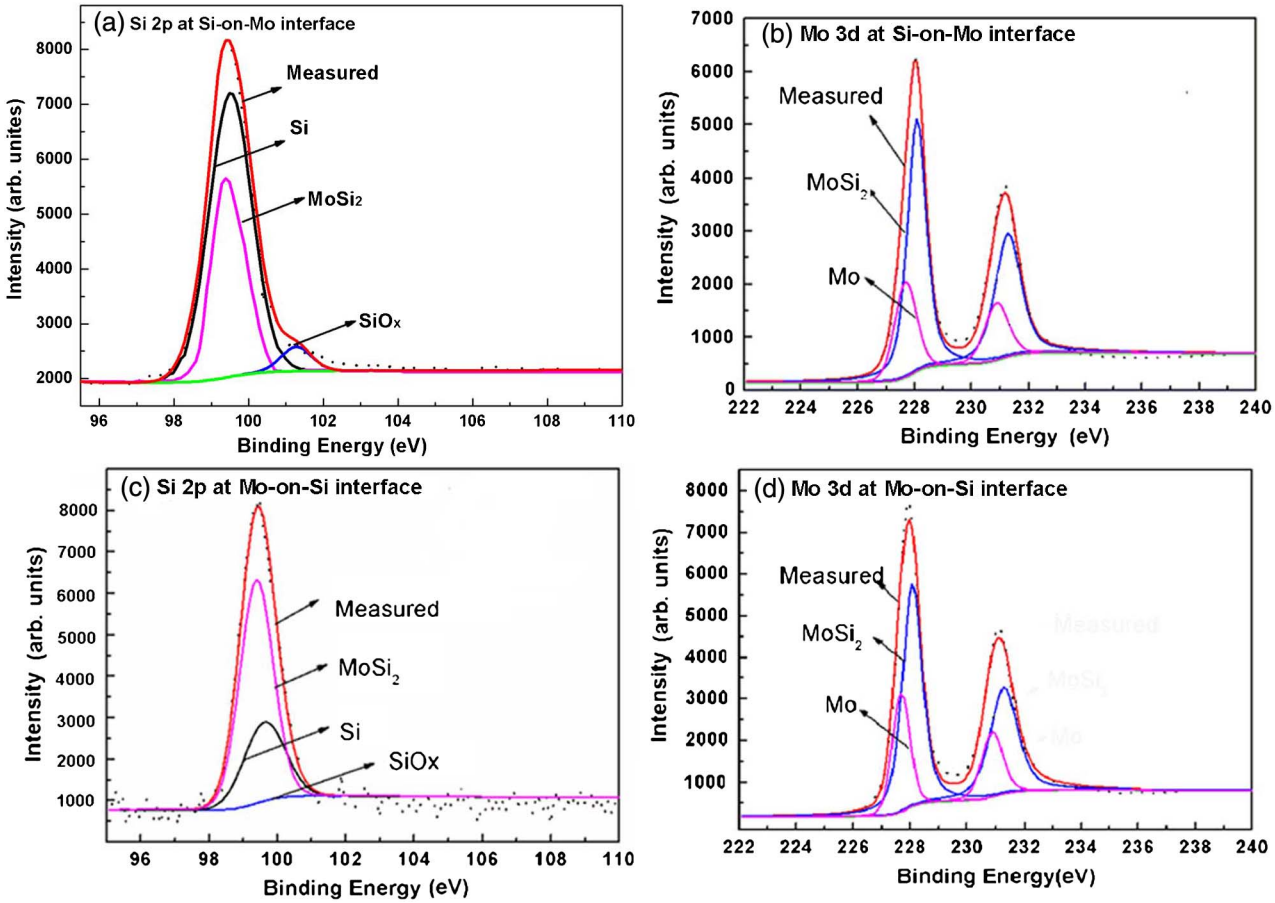

Fig. 3. Regional XPS scan of (a) Si 2p and (b) Mo 3d at the Si-on-Mo interface; (c) Si 2p and (d) Mo 3d at the Mo-on-Si interface.

and the interfaces are not contaminated with oxygen with our deposition conditions. According to the results in Ref. [20], the contaminant (O) was accumulated at the interface. However, an accurate speed control system is equipped in our magnetron sputtering system to adjust the rotation speed on a nondeposition range; accumulation of O at the interface is significantly reduced. Furthermore, a very low base pressure was supplied to reduce the oxygen level in the deposition chamber so the contaminant (O) can be avoided in multilayer coatings.

Cross-sectional structure is observed by HRTEM, as shown in Fig. 4(a). The interface is clear and the thickness is uniform. From the cross-sectional profile curve in Fig. 4(b), the average periodic thickness is about 70.68 Å.

Table 1. XPS Photoelectron Curve Fitting Results

Item	Si 2p		Mo $3d_{5/2}$	Mo $3d_{3/2}$
Charge	Si^{2-}	Si^{+2x}	Mo^{4+}	Mo^{4+}
Composition	$MoSi_2$	SiO_x	$MoSi_2$	$MoSi_2$
B. E. S. (eV)	99.4	102.5	228.1	231.3
B. E. M. (eV)	99.4	101.3	228.1	231.3

B. E. S. binding energy for the Si-on-Mo interface
B. E. M. binding energy for the Mo-on-Si interface

The thickness of the Mo layer is about 24.10 Å and the Si layer is about 40.61 Å [Fig. 4(c)], which are close to the designed thickness. The Mo-on-Si interlayer is about 3.15 Å and the Si-on-Mo interlayer is about 2.62 Å. This indicates that the thickness of Mo/Si multilayer is controlled precisely in our magnetron sputtering system. The periodic thickness obtained from HRTEM agrees well with the GIXRR fitted results.

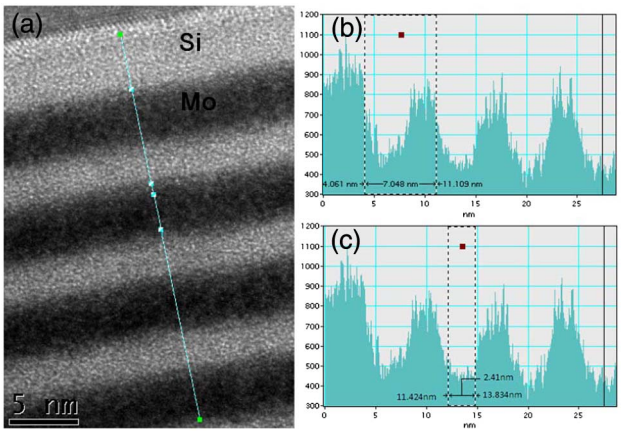

Fig. 4. (a) HRTEM image for the cross-sectional structure of the Mo/Si multilayer; (b) the cross–sectional profile curve; (c) the Mo layer thickness.

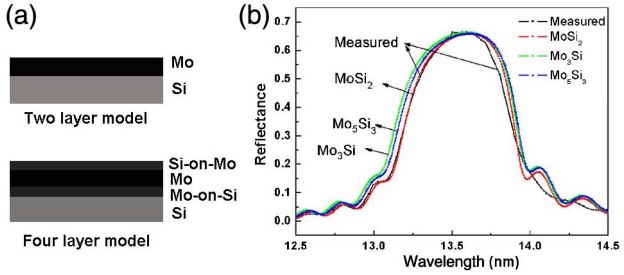

Fig. 5. (a) Two-layer and four-layer models; (b) the calculated reflectivity of the Mo/Si multilayers with $MoSi_2$ interlayer compounds using the four-layer model.

Table 2. EUV Reflective Calculated Results Units: Å

Interlayer	d_{Mo}	d_{Si}	d_1	d_2	σ_{Mo}	σ_{Si}	σ_1	σ_2
$MoSi_2$	24.10	40.61	3.15	2.62	0.11	0.6	1.09	0.25
Mo_5Si_3	23.09	40.17	3.75	3.69	0.88	0.56	0.7	1.01
Mo_3Si	22.52	40.28	3.18	4.68	1.12	1.01	0.22	0.51

According to the XPS results, the main composition at both interfaces of the multilayer is $MoSi_2$. In order to get the accurate interlayer width and confirm the composition at both interfaces, the reflectivity spectrum at 13.5 nm is calculated by a four-layer model [Fig. 5(a)]. Mo_3Si, Mo_5Si_3, and $MoSi_2$ are regarded as interlayer compounds to calculate the measured reflectivity curve. As shown in Fig. 5(b), compared to Mo_3Si and Mo_5Si_3, the calculated curve that takes $MoSi_2$ as an interlayer formation matches the measured data best. That is to say, $MoSi_2$ is the main silicon compound at both interfaces. The initial multilayer structure that is used do the EUV reflectivity calculation is extracted from HRTEM results. The calculated parameters are listed in Table 2. In Table 2, d_1 and d_2 are the Mo-on-Si and the Si-on-Mo interlayer thickness, respectively; σ is the corresponding roughness of each layer.

In this Letter, an Mo/Si multilayer with a reflectivity up to 65% at 13.5 nm is fabricated for the interface study. Uniform multilayer thickness is confirmed by GIXRR results and the multilayer profile is observed by HRTEM, which indicate that the thickness of the Mo/Si multilayer is controlled precisely with our coating system. XPS results indicate that oxygen contamination due to the silicon oxidation is only found at the surface and not at the interlayer. According to the XPS peak fitting results, $MoSi_2$ is the main composition on both the interfaces. Considering $MoSi_2$ as the interlayer formation, the calculated reflectivity by the four-layer model fits best with the reflectivity curve at 13.5 nm. Further study of the interface engineer is needed to improve the interface quality and enhance the optical performance.

This work was supported by the International Science & Technology Cooperation Program of China (No. 2012DFG51590) and the National Natural Science Foundation of China (No. 11304328).

References

1. B. Wu and A. Kumar, Appl. Phys. Rev. **1**, 011104 (2014).
2. S. Yi, B. Mu, X. Wang, J. Zhu, L. Jiang, Z. Wang, and P. He, Chin. Opt. Lett. **12**, 013401 (2014).
3. Y. Li, H. Zhang, H. Wang, F. He, X. Wang, Y. Liu, and J. Cao, Appl. Surf. Sci. **317**, 902 (2014).
4. S. Yulin, N. Benoit, T. Feigl, and N. Kaiser, Microelectron. Eng. **83**, 692 (2006).
5. T. Feigl, S. A. Yulin, N. Kaiser, and R. Thielsch, Proc. SPIE **3997**, 420 (2000).
6. J. L. Zhao, K. Yi, H. Wang, M. Fang, B. Wang, G. Hu, and H. B. He, Thin Solid Films **592**, 256 (2015).
7. J. G. Hu, Q. W. Li, X. D. Lin, Y. Liu, J. H. Long, L. Y. Wang, and H. B. Tang, Chin. Opt. Lett. **12**, 072201 (2014).
8. S. L. Nyabero, R. W. E. van de Kruijs, A. E. Yakshin, and F. Bijkerk, Appl. Phys. Lett. **103**, 093105 (2013).
9. P. V. Satyam, A. K. Balamurugan, A. K. Tyagi, and N. C. Das, Appl. Surf. Sci. **214**, 259 (2003).
10. M. Nayak, G. S. Lodha, R. V. Nandedkar, S. M. Chaudhari, and P. Bhatt, J. Electron Spectrosc. Relat. Phenom. **152**, 115 (2006).
11. M. G. Sertsu, M. Nardello, A. Giglia, A. J. Corso, C. Maurizio, L. Juschkin, and P. Nicolosi, Appl. Opt. **54**, 10351 (2015).
12. D. L. Windt, Comput. Phys. **12**, 360 (1998).
13. S. Bajt, D. G. Stearns, and P. A. Kearney, J. Appl. Phys. **90**, 1017 (2001).
14. A. Neuhold, S. Fladischer, S. Mitsche, H. G. Flesch, A. Moser, J. Novak, and R. Resel, J. Appl. Phys. **110**, 114911 (2011).
15. S. Bruijn, R. W. E. Van de Kruijs, A. E. Yakshin, and F. Bijkerk, Defect Diffus. Forum **283**, 657 (2009).
16. S. Yulin, T. Feigl, T. Kuhlmann, N. Kaiser, A. I. Fedorenko, V. V. Kondratenko, O. V. Poltseva, V. A. Sevryukova, A. Y. Zolotaryov, and E. N. Zubarev, J. Appl. Phys. **92**, 1216 (2002).
17. G. P. Halada, C. R. Clayton, H. Herman, S. Sampath, and R. Tiwari, J. Electrochem. Soc. **142**, 74 (1995).
18. J. M. Slaughter, A. Shapiro, P. A. Kearney, and C. M. Falco, Phys. Rev. B **44**, 3854 (1991).
19. C. D. Wagner, D. E. Passoja, H. F. Hillery, T. G. Kinisky, H. A. Six, W. T. Jansen, and J. A. Taylor, J. Vac. Sci. Technol. **21**, 933 (1982).
20. S. Deng, H. Qi, K. Yi, Z. Fan, and J. Shao, Appl. Surf. Sci. **255**, 7434 (2009).